5-3-2012

Gravity Wave Propagation in a Diffusively Separated Gas: Effects on the Total Gas

Michael P. Hickey Ph.D.
Embry-Riddle Aeronautical University, hicke0b5@erau.edu

R. L. Walterscheid
Space Science Applications Laboratory

Scholarly Commons Citation

Citation: Walterscheid, R. L., and M. P. Hickey (2012), Gravity wave propagation in a diffusively separated gas: Effects on the total gas, J. Geophys. Res., 117, A05303, doi: https://doi.org/10.1029/2011JA017451

Gravity wave propagation in a diffusively separated gas: Effects on the total gas

R. L. Walterscheid[1] and M. P. Hickey[2]

Received 15 December 2011; revised 13 February 2012; accepted 6 March 2012; published 3 May 2012.

[1] We present a full-wave model that simulates acoustic-gravity wave propagation in a binary-gas mixture of atomic oxygen and molecular nitrogen, including molecular viscosity and thermal conductivity appropriately partitioned between the two gases. Compositional effects include the collisional transfer of heat and momentum by mutual diffusion between the two gases. An important result of compositional effects is that the velocity and temperature summed over species can be significantly different from the results of one-gas models with the same height dependent mean molecular weight (M(z)). We compare the results of our binary-gas model to two one-gas full-wave models: one where M is fixed and fluctuations of M (M′) are zero and the other where M is conserved following parcel displacement (whence M′ is nonzero). The former is the usual approach and is equivalent to assuming that mutual diffusion acts instantaneously to restore composition to its ambient value. In all cases we considered, the single gas model results obtained assuming that M is conserved following parcels gave significantly better agreement with the binary-gas model. This implies that compositional effects may be included in one-gas models by simply adding a conservation equation for M and for the specific gas at constant pressure, which depends on M.

Citation: Walterscheid, R. L., and M. P. Hickey (2012), Gravity wave propagation in a diffusively separated gas: Effects on the total gas, *J. Geophys. Res.*, *117*, A05303, doi:10.1029/2011JA017451.

1. Introduction

[2] A widely used simplification in dynamical models of the diffusively stratified thermosphere is the application of equations for a single gas (the total gas) with height-dependent physical properties such as mean molecular weight and specific heats. A further approximation is that composition remains fixed at a fixed location despite the advection of one-gas species relative to another [e.g., *Richmond and Matsushita*, 1975; *Fuller-Rowell and Rees*, 1981; *Mikkelsen et al.*, 1981; *Walterscheid et al.*, 1985; *Mikkelsen and Larsen*, 1991; *Brinkman et al.*, 1995; *Hagan et al.*, 1999]. This approximation is used in lieu of the much more complicated and computationally intensive system of equations that must be solved when a multiconstituent approach is used [e.g., *Colegrove et al.*, 1966; *Hays et al.*, 1973; *Reber and Hays*, 1973; *Straus et al.*, 1977; *Mayer et al.*, 1978; *Mayr et al.*, 1984, 1987; *Del Genio et al.*, 1979a, 1979b; *Dickinson et al.*, 1984; *Sun et al.*, 1995]. A general result is that motion (primarily vertical motion) drives a diffusively separated atmosphere with height-dependent composition out of diffusive equilibrium and causes composition to be locally perturbed. The standard one-gas models assume implicitly that such advective perturbations are instantaneously annulled by mutual diffusion [*Walterscheid and Hickey*, 2001].

2. Theory

[3] In this work we consider a binary mixture of atomic oxygen and molecular nitrogen. Since the molecular weights of N_2 and O_2 are similar (28 versus 32) the binary mixture comprising O and N_2 is not too different from a binary mixture of O and $N_2 - O_2$.

2.1. Two-Gas Collisionally Coupled System

[4] We develop a full-wave model to simulate acoustic-gravity wave fluctuations in a binary gas. It includes all the processes currently included in the one-gas full-wave model, and also includes the diffusion of heat and momentum between the two constituents. The linearized equations for a two constituent atmosphere that includes the collisional transfer of heat and momentum between constituents are given by *Del Genio* [1978]. We generalize these equations by including the molecular diffusion of heat and momentum. The viscous stress tensor is

$$\underline{\sigma}_{ij} = -\mu\left\{\frac{\partial v_i}{\partial x_j} + \frac{\partial v_j}{\partial x_i} - \frac{2}{3}\,\delta_{ij}\frac{\partial v_i}{\partial x_i}\right\} \tag{1}$$

where μ is the coefficient of molecular viscosity, v_i is the i-th velocity component and δ_{ij} is the Kronecker delta. The heat and momentum equations for the two constituents are

[1]Space Science Applications Laboratory, The Aerospace Corporation, El Segundo, California, USA.
[2]Department of Physical Sciences, Embry-Riddle Aeronautical University, Daytona Beach, Florida, USA.

0148-0227/12/2011JA017451

collisionally coupled. Assuming hard elastic spheres and a Maxwellian velocity distribution for each species results in the following expression for the coupling coefficient K_{st} [*Burgers*, 1969; *Schunk*, 1977; *Del Genio*, 1978]

$$K_{st} = \frac{8}{3}\sigma^2 \bar{n}_s \bar{n}_t \left(\frac{2\pi m_s m_t k \bar{T}}{m_s + m_t}\right)^{1/2} \tag{2}$$

where σ is the sum of the radii of the colliding spheres, m is the molecular mass, n is the number density, k is Boltzmann's constant, and T is temperature. Subscripts refer to individual species and the overbar refers to a basic state quantity. Dividing K_{st} by the basic state mass density ρ_s gives a collision frequency, where the subscript s refers to the gas to which the prognostic equation for momentum or heat applies.

2.2. Viscosity and Thermal Conduction

[5] The coefficients of thermal conduction and dynamic viscosity for one species are not independent of the other species. This is because these coefficients are proportional to the mean free path and the mean free path is inversely proportional to the total number density and the square of the effective molecular diameter for the mixture [*Kittel*, 1969]. The viscosity for a single gas derived from kinetic theory is

$$\eta_i = \frac{1}{3} M_i n_i \bar{c}_i l_i = \frac{M_i \bar{c}_i}{3\pi d_i^2} \tag{3}$$

where the subscript i refers to the $i - th$ constituent, M_i is the molecular weight, $\bar{c}_i$ is the mean particle speed, l_i is the mean free path, d_i is the molecular diameter and n_i is the number density. For a single gas $l_i = (\pi d_i^2 n_i)^{-1}$. For a mixture of gases $l_i = (\pi d_{eff}^2 N)^{-1}$, whence

$$\eta_i^* = r_i \frac{d_i^2}{d_{eff}^2} \eta_i \tag{4}$$

where $r_i = n_i/N$, N is total number density and d_{eff} is the effective molecular collision diameter of the i-th species with respect to the mixture. The factor r_i ranges over a much larger range of values than the diameter factor and we apply the simple formula

$$\eta_i^* = r_i \eta_i \tag{5}$$

This is consistent with the widely used semi-empirical equation obtained by *Herning and Zipperer* [1936] for the viscosity of a gas mixture.

2.3. Prognostic Equation for the Mean Molecular Weight

[6] *Walterscheid and Hickey* [2001] showed that following the motion the mean molecular weight M in a gas mixture varies in time according to

$$\frac{D \log M}{Dt} = \frac{1}{N} \sum_j \nabla \cdot \mathbf{\Phi}_j \tag{6}$$

where

$$\mathbf{\Phi}_j = n_j \mathbf{u}_j - n_j \mathbf{u} \tag{7}$$

and where the subscripts denote individual species and $\mathbf{u}$ is the mass density weighted fluid velocity. The linearized form of (6) is

$$\frac{\partial}{\partial t}\frac{M'}{\bar{M}} = -w' \frac{d \log \bar{M}}{dz} + \frac{1}{\bar{N}} \sum_j \nabla \cdot \mathbf{\Phi}'_j \tag{8}$$

where $\mathbf{\Phi}'_j = \bar{n}_j \mathbf{u}''$ and where $\mathbf{u}'' = \mathbf{u}'_j - \mathbf{u}'$ is the perturbation diffusion velocity for the $j - th$ constituent. It is easily shown that

$$\begin{aligned} \mathbf{u}''_O &= \bar{r}_{N_2}(\mathbf{u}'_O - \mathbf{u}'_{N_2}) \\ \mathbf{u}''_{N_2} &= \bar{r}_O(\mathbf{u}'_{N_2} - \mathbf{u}'_O) \end{aligned} \tag{9}$$

where $\bar{r}_i$ is the basic state mass density mixing ratio of the i-th species. In the limit of fast diffusion the terms on the right side of (8) balance and

$$\frac{\partial}{\partial t}\frac{M'}{\bar{M}} = 0 \tag{10}$$

that is, the motion does not perturb the mean molecular weight profile ($M' = 0$). In the limit of slow diffusion the effects of mutual diffusion are too slow to balance the perturbing effects of the vertical motion. This gives

$$\frac{\partial}{\partial t}\frac{M'}{\bar{M}} = -w' \frac{d \log \bar{M}}{dz} \tag{11}$$

Equation (11) is just the linearized equivalent of $DM/Dt = 0$.

3. Simulations

[7] To elucidate multiconstituent effects on the total gas we perform simulations with our binary-gas model and one-gas model.

3.1. One-Gas Full-Wave Model

[8] The full-wave model is a linear, steady state model that describes the vertical propagation of acoustic-gravity waves in an atmosphere with molecular viscosity and thermal conduction, ion drag, Coriolis force, and the eddy diffusion of heat and momentum in the mesosphere. Here we ignore ion drag, the Coriolis force and eddy diffusion. The model solves the Navier-Stokes equations on a high resolution vertical grid subject to boundary conditions, and allows quite generally for propagation in a height varying atmosphere (non-isothermal mean state temperature and height varying mean winds and diffusion). The model has been described by *Hickey et al.* [1997], *Walterscheid and Hickey* [2001], and *Schubert et al.* [2003].

[9] The linearized equations are numerically integrated from the lower to the upper boundary using the tridiagonal algorithm described by *Bruce et al.* [1953] and *Lindzen and Kuo* [1969]. The lower boundary is set well below the region of interest and a lower sponge layer is implemented to avoid the extraneous effects of wave reflection build up below the region of interest [e.g., *Hickey et al.*, 2000]. In this study we employ a lower sponge layer with the lower boundary placed 450 km below zero altitude. The large depth is required to allow the damping to increase gradually to avoid undue reflection from gradients in the damping rate.

[10] The wave forcing is then through the addition of an inhomogeneous heat term in the energy equation defined by a Gaussian heating profile over altitude, with a full-width-at-half-max of 0.125 km. It is centered at an altitude of 80 km. We adjust the source amplitude to give reasonable peak amplitudes.

[11] At the upper boundary (here 650 km altitude) a radiation condition is imposed using a dispersion equation that includes dissipation [*Hickey and Cole*, 1987]. A Rayleigh-Newtonian sponge layer in addition to the natural absorption by viscosity and heat conduction is also implemented to absorb waves reflected from the upper boundary [*Hickey et al.*, 1997; *Walterscheid and Hickey*, 2001; *Schubert et al.*, 2003]. The Rayleigh coefficient is given as

$$K_R(z) = \Omega_L \exp((z_L - z)/H_L) + \Omega_U \exp((z - z_U)/H_U) \quad (12)$$

Here, $\Omega = \omega - \mathbf{k}\cdot\bar{\mathbf{u}}_H$ is the wave intrinsic frequency, ω is the wave frequency, $\mathbf{k}$ is the wave number vector, and $\bar{u}_H$ is the mean horizontal wind vector. Also, z_L and H_L are the altitude and characteristic decay height associated with the lower sponge, while the upper sponge is similarly defined with subscript "u." Here z_L and z_U were set to the lower and upper boundary altitudes, respectively. The Newtonian cooling coefficient has the identical form. The mean molecular weight is a specified function of altitude.

[12] The model can be run in two modes. One employs the usual approach where (10) is prescribed. The other adds an equation for wave perturbed M, namely (11). This is described by *Walterscheid and Hickey* [2001]. These authors suggested that the latter approach was more accurate. We shall address this suggestion with the binary-gas model.

3.2. Binary-Gas Model

[13] The linearized equations are numerically integrated from the lower to the upper boundary using the approach described in the preceding section. The equations for the two coupled species are solved simultaneously. The heating is apportioned between the two species so that the total heating is the same as for the one-gas full-wave model and so that the heating rate for each species in units of $K\ s^{-1}$ is the same. This is done by prescribing the N_2 forcing to be a factor C_{N_2}/C_O greater than the O forcing, where $C = \rho c_p$ is the heat capacity.

3.3. Binary Total Gas Model

[14] The results of one-gas full-wave simulations are not equivalent to the results obtained when the results of multi-constituent models are summed. This follows from the fact that neither (10) nor (11) are rigorously true. To obtain the total gas response based on the results of the two-gas model we combine the velocity components by mass density weighting and the temperature by heat capacity weighting. Our "binary total gas" model is just the results of the two-gas model summed in this manner.

3.4. Basic State

[15] In order to simplify interpretation in terms of compositional effects without the complications of wave reflection we perform most of our calculations with an isothermal basic state. Some concluding simulations are performed with a realistic nonisothermal basic state. All simulations involve a resting basic state.

[16] The basic state is defined by the MSIS-90 model [*Hedin*, 1991] evaluated at the equator for a longitude of 105°W and for a UT of 09 h and day number 318. The solar and geomagnetic conditions were assumed to be low, with the daily $F_{10.7} = 99$, the 81-day mean $F_{10.7} = 120$, $a_p = 38$ and year = 1993.

[17] Basic state profiles of mean molecular weight, and collision coefficients for N_2 through O and O through N_2 are shown in Figure 1. The strongest compositional gradient occurs in the lower thermosphere between ~150 and 230 km.

3.4.1. Isothermal Basic State

[18] The isothermal basic state is based on the MSIS-90 model as described above. We adopt a temperature (634.1 K) that is equal to the average of the temperatures obtained at altitudes of 120 km and 500 km, respectively. The mean pressure obtained at an altitude of 120 km is chosen as a reference, and the N_2 and O pressure distributions (and the N_2 and O number densities) are each calculated based on the assumption of diffusive equilibrium and integrating the barometric equation using a constant scale height for each. From the mean pressure and temperature the mean density is calculated using the ideal gas equation of state.

[19] The collision frequencies (shown in Figure 1) diminish as number density with increasing altitude. The collision frequency for O in N_2 diminishes more rapidly than N_2 in O because the former is proportional to N_2 number density while the latter is proportional to O number density, and N_2 diminishes more rapidly with altitude than O.

3.4.2. Nonisothermal Basic State

[20] The temperature is given by the MSIS-90 model at altitudes above 120 km, with a mean exospheric temperature of 877 K. At lower altitudes the temperature is forced to become isothermal, smoothly decreasing to a value of 240 K at low altitudes. Using the pressure at 120 km altitude as a reference, the pressures at other altitudes are obtained by assuming diffusive equilibrium and integrating the barometric equation using the local scale height values for N_2 and O. The mass density and number density are then calculated using the ideal gas equation of state for N_2 and O.

3.5. Model Calculations

[21] We perform two sets of calculations for identical background states and total forcing. One set is based on our one-gas full-wave model; the other is based on the binary-gas model. In the latter case we sum the constituents, appropriately weighted as described before, to form results that can be compared to the one-gas model. The main goal of this study is to compare the two different formulations of the one-gas results with the binary total-gas model and elucidate the differences.

[22] The one-gas model is run in two modes. The first is to keep the mean molecular weight locally fixed according to (10) and the other is to allow the vertical motion to perturb the mean molecular weight according to (11). We also include a similar equation describing the conservation of the specific heat at constant pressure (c_p) since this depends on M. See *Walterscheid and Hickey* [2001] for details.

[23] Simulations are performed for three wave periods (10, 20 and 40 min) and three horizontal wavelengths (60,

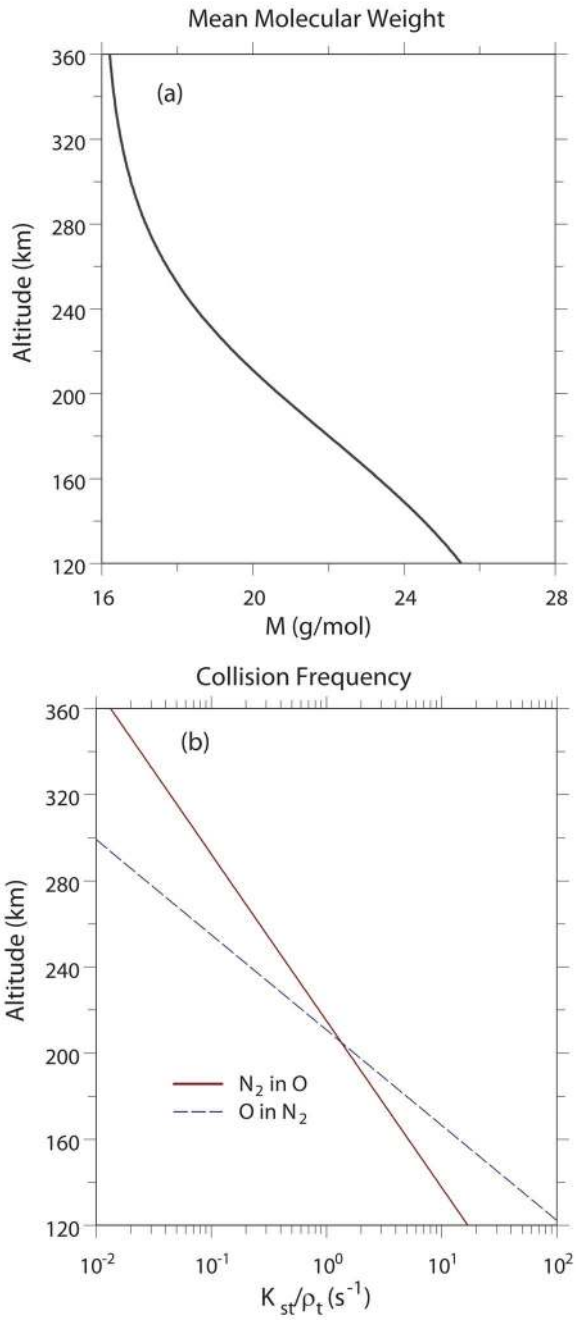

Figure 1. Basic state profiles of (a) mean molecular weight and (b) collision coefficients for N_2 through O (solid) and O through N_2 (dashed).

120 and 240 km). Thus all waves have a horizontal phase velocity $c = 100\ m\ s^{-1}$, while covering a range of frequencies. The phase speed is fast enough to give vertical wavelengths that are long enough to avoid strong scale-dependent dissipation low in the thermosphere and allow penetration of the wave into the region of the thermosphere where composition gradients are largest.

4. Results

[24] All results are for the isothermal atmosphere described in section 3.4.1 except as noted. Figure 2 shows vertical profiles of the amplitude of the two-gas model predictions of the vertical diffusion velocities for O, N_2 and the total gas vertical velocity for a wave with a period of 10 min and a horizontal wavelength of 60 km. In the lower thermosphere the two constituents are very tightly coupled and the diffusion velocities are very small with the O diffusion velocity w''_O being the greater, reflecting the fact that the less dense of the two species must have the larger diffusion velocity (see (9)). The diffusion velocity w''_O grows rapidly with altitude; then growth diminishes until a peak is reached near ~210 km. The diffusion velocity for w''_{N_2} grows even more rapidly, and peaks ~20 km higher than w''_O. This

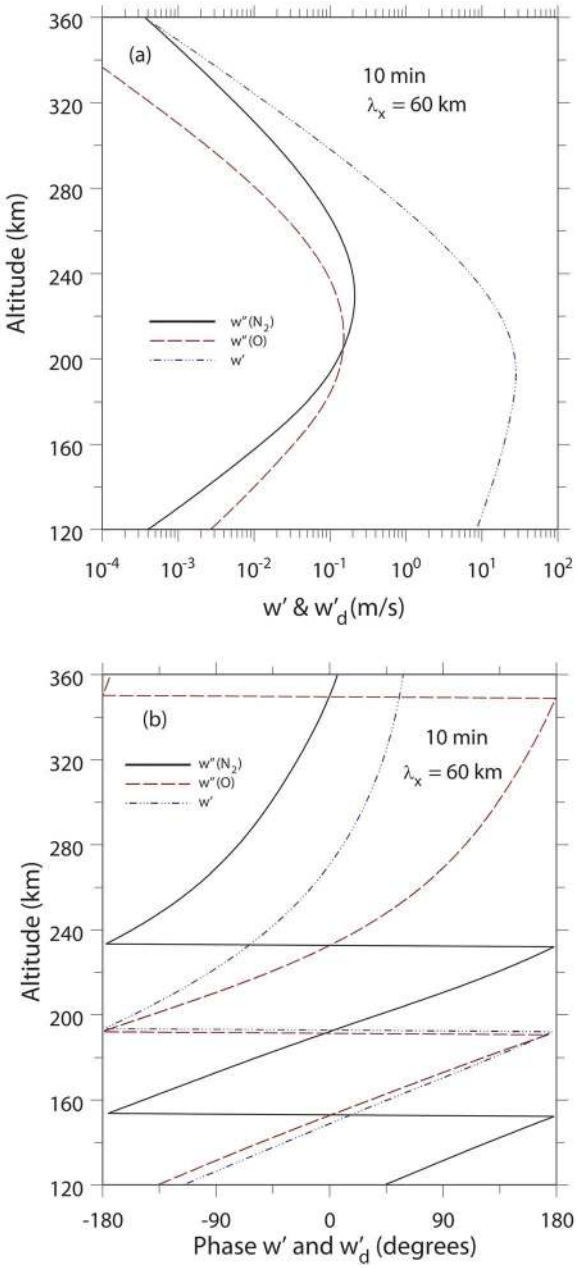

Figure 2. Binary-gas model predictions of wave (a) amplitudes and (b) phase of the total gas vertical velocity w' and the individual O and N_2 diffusion velocities $w''_j = w'_j - w'$ for a wave with a period of 10 min and horizontal wavelength of 60 km: w', dash dotted; w''_O, dashed; w''_{N_2}, solid.

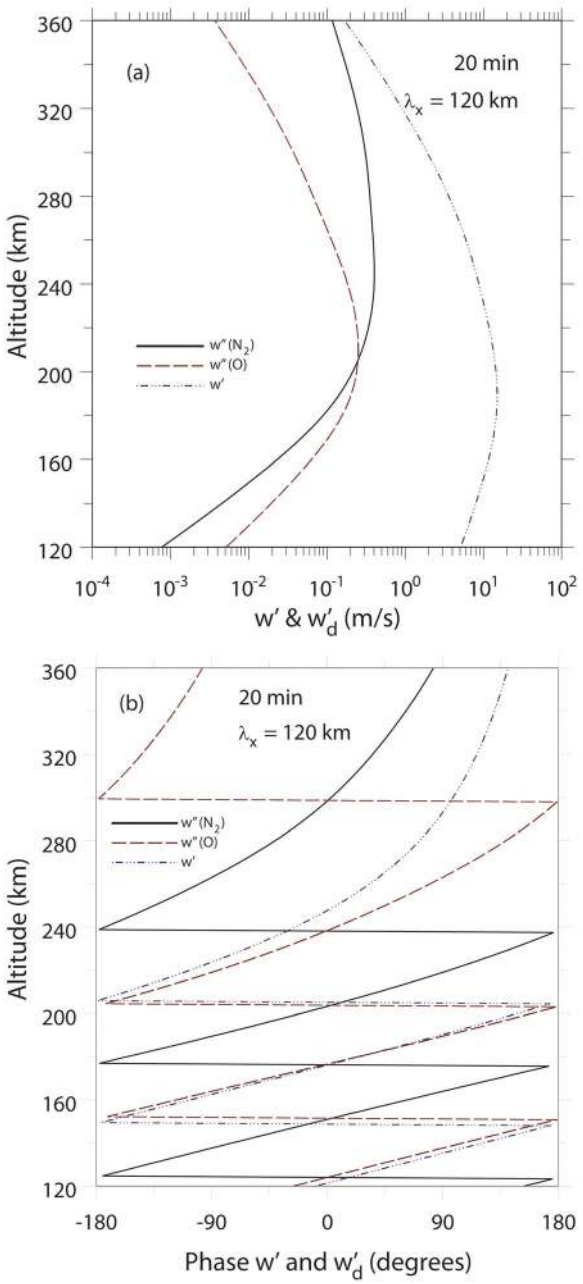

Figure 3. Same as Figure 2 except for a wave with a period of 20 min and horizontal wavelength of 120 km.

reflects both the decreasing abundance of N_2 relative to O and the related fact that viscosity and thermal conductivity for N_2 diminishes as its basic state number density mixing ratio diminishes (see (5)). The total gas vertical velocity w' peaks near 210 km. Thus the total wave peaks near the top of the region where the steepest decreases in mean molecular weight are found (see Figure 1a). The diffusion velocities grow with altitude relative to w' as the coupling between the two species diminishes. Near 360 km altitude w''_{N_2} becomes comparable to w'.

[25] Below ~200 km the phases of w''_O and w' are nearly equal indicating that $w'_O > w'_{N_2}$ and that $w' \approx w'_O$ because of the tight coupling that exists in the lower thermosphere. The phase difference between w''_O and w' diverges as the species decouple and O becomes the dominant species. The phases of w''_O and w''_{N_2} are in antiphase throughout in agreement with (9).

[26] Figure 3 shows the same quantities as in Figure 2 but for a wave with a period of 20 min and horizontal wavelength of 120 km. The results are similar to those shown in Figure 2, but the w' and w''_O profiles peak lower by about 20 km and the amplitude of w''_{N_2} diminishes more slowly above a broad maximum between ~220 and 300 km. The phases are similar to those shown in Figure 2, except for a phase offset and phase gradients indicating shorter vertical wavelengths.

[27] Figure 4 shows the same quantities as in Figure 2 but for a wave with a period of 40 min and horizontal wavelength of 240 km. The results continue the trend from Figure 2 to Figure 3, with the w' and w''_O profiles peaking lower and the tendency for w''_{N_2} above ~240 km toward constant amplitude with altitude. The w''_{N_2} profile does not have a distinct peak. Amplitude growth diminishes until it becomes essentially constant or slightly increasing above about 260 km. This reflects an overall tendency for slower amplitude decreases above the peak as period increases, on the one hand, and the increase of w''_{N_2} relative to w''_O, on the other. The corresponding phases are similar to Figures 2 and 3, but are shifted and the vertical wavelengths are shorter. The shorter vertical wavelengths imply greater dissipation due to viscosity and thermal conduction.

[28] Figure 5 shows vertical profiles of the amplitudes of contributions to the relative mean molecular weight fluctuation from vertical advection and mutual diffusion (respectively, the first and second terms on the right of (8)) for a wave with a 10 min period and 60 km horizontal wavelength. The contributions are calculated from the binary-gas model. Throughout the lower thermosphere mutual diffusion is negligible compared to vertical advection, reflecting the tight coupling between species (small diffusion velocities). Above ~240 km the diffusive contribution begins to affect the $M'/\bar{M}$ profile, but at these altitudes the amplitude of $M'/\bar{M}$ is less by about an order of magnitude from its peak value of ~1%. The phases of $M'/\bar{M}$ and of the advective contribution are nearly equal through the lower thermosphere reflecting the strong dominance of vertical advection over mutual diffusion. Above 220 km the phases diverge somewhat reflecting the growing contribution from mutual diffusion.

[29] Figure 6 is the same as Figure 5 except for a wave with a 20 min period and horizontal wavelength of 120 km. The results are similar to those shown in Figure 5 except that mutual diffusion effects become evident at lower altitudes, reflecting the fact that diffusion effects have longer to act to diminish the M' perturbations established by vertical advection. The phases are similar to those shown in Figure 5.

[30] Figure 7 shows the same results for a 40 min wave with a horizontal wavelength of 2400 km. The results continue the trend established by the two shorter period waves. The effect of mutual diffusion is appreciable starting at altitudes near 200 km. By 360 km (the highest altitude plotted) the reduction due to mutual diffusion in the value of $M'/\bar{M}$ induced by vertical advection is a factor of ~2. The phases are similar to those shown in Figures 5 and 6.

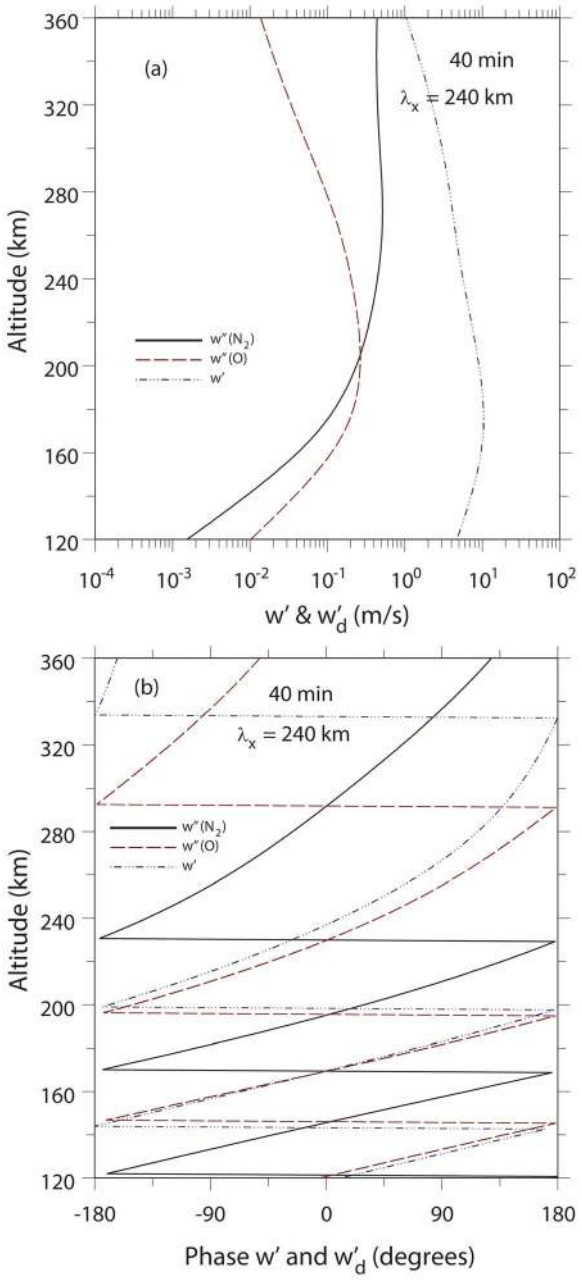

Figure 4. Same as Figure 2, but for a wave with 40 min period and 240 km wavelength.

[31] We now examine the effects of composition on the total gas. Compositional effects enter the governing equations primarily through the ideal gas law, adding a term $M'/\bar{M}$ and through the first law adding a term proportional to $c_p'/\bar{c}_p$ [*Walterscheid and Hickey*, 2001]. Both affect the thermal response and we examine compositional effects on the total gas by examining the effects on temperature.

[32] Figure 8 shows the amplitude of the relative temperature fluctuation for a 10 min wave with a horizontal wavelength of 60 km. Results are from the one-gas model for the $M' = 0$ limit (10), from the one-gas model with where M' is nonzero based on the $DM/Dt = 0$ limit (11), and from the binary total gas model. Over the whole domain plotted the results based on $DM/Dt = 0$ are much closer to the binary total gas results than are the results for the $M' = 0$ limit; the agreement in the former case being essentially exact. The results with $M' = 0$ (the standard approximation) are significantly less accurate. Where $T'/\bar{T}$ peaks (near 180 km) the error is close to 30%. The phases for the binary total gas results and for the $DM/Dt = 0$ limit agree very closely over all attitudes shown. The phases for the $M' = 0$ result are

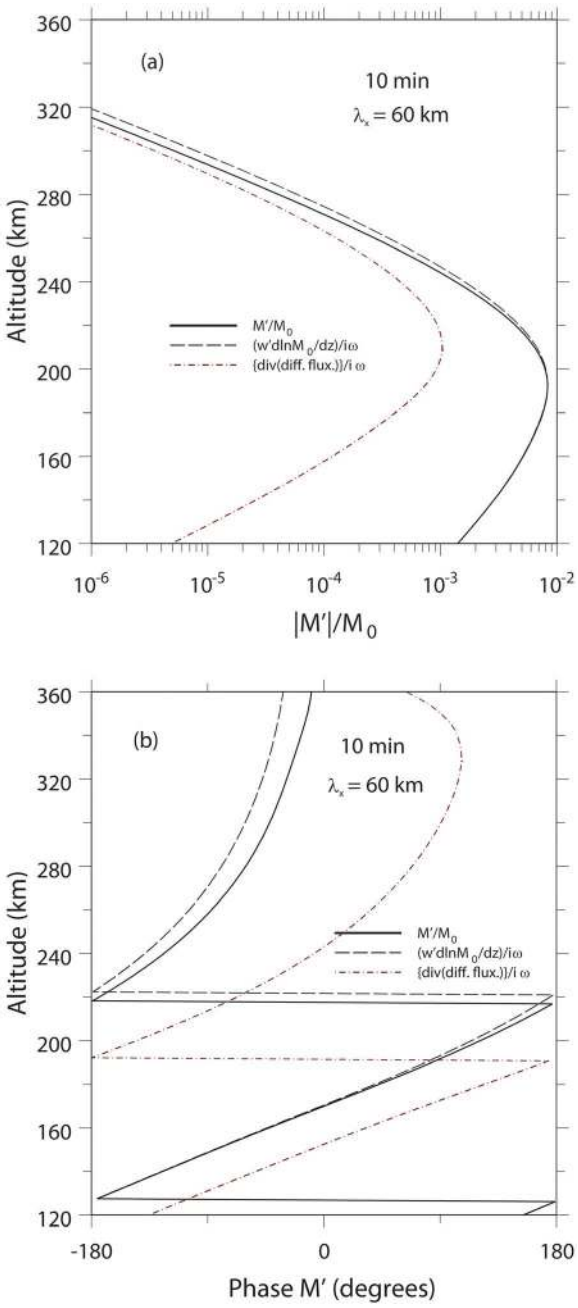

Figure 5. Vertical profiles of the contributions to the relative mean molecular weight fluctuation (solid) from vertical advection (long dashed) and mutual diffusion (dotted) for wave with a 10 min period and 60 km horizontal wavelength based on the binary-gas model. Quantities plotted are amplitudes. (a) Amplitude and (b) phase.

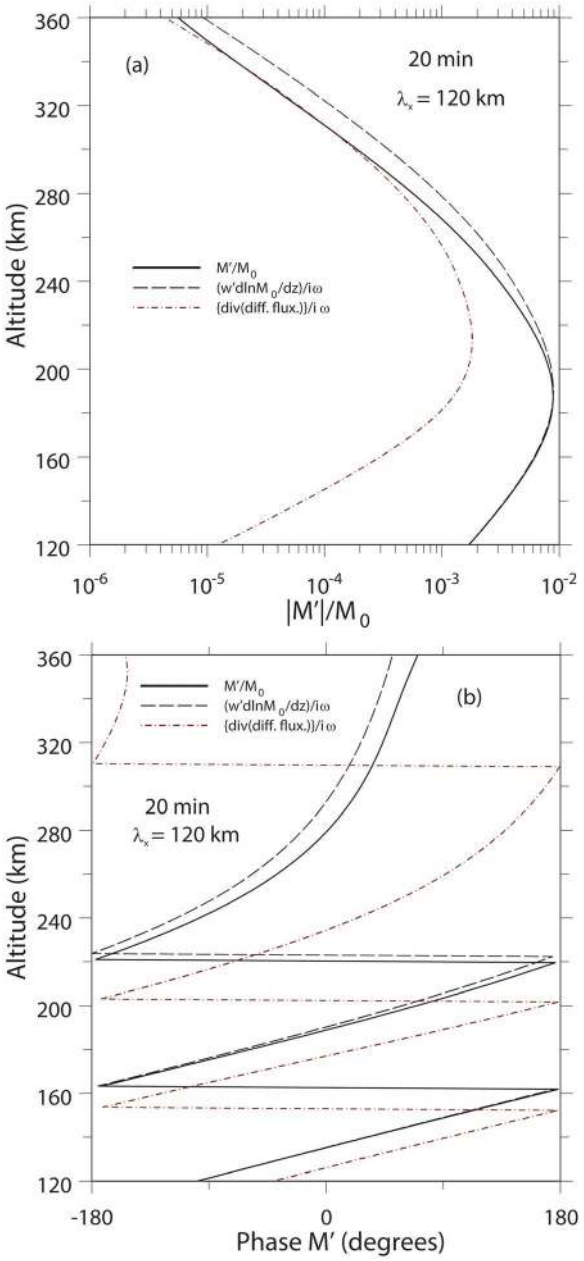

Figure 6. Same as Figure 5 except for a wave with a 20 min period and 120 km horizontal wavelength.

significantly different from the other results, the phase difference being ∼15° at 120 km, growing to ∼60° by 360 km.

[33] Figure 9 is the same as Figure 8 except for 20 min wave with a 120 km horizontal wavelength. The results are similar, except that the wave peaks slightly lower (∼10 km) and the effects of mutual diffusion are somewhat greater, but not significant. The phase differences between the various solutions are similar to those seen in Figure 8.

[34] Figure 10 is the same as Figure 8 except for a 40 min wave with a 240 km horizontal wavelength. The wave peaks about 20 km lower than the 20 min wave and the resultant $M'/\bar{M}$ wave shows a greater contribution from the effects of mutual diffusion, though the dominant contribution comes from vertical advection. The greater contribution from mutual diffusion is seen in the phases, where the phase difference between the $M' = 0$ solution and the other two is decreased.

[35] Figure 11 shows the amplitude of the relative temperature fluctuation for a 10 min wave with a horizontal wavelength of 60 km for the nonisothermal atmosphere described in section 3.4.2. The results are similar to the isothermal results (Figure 8) except that the wave peaks lower by ∼20 km and the differences between the $M' = 0$ solution and the more accurate solutions are reduced to ∼20%. This is consistent with the wave peaking lower so that the main effects of vertical advection are weighed to

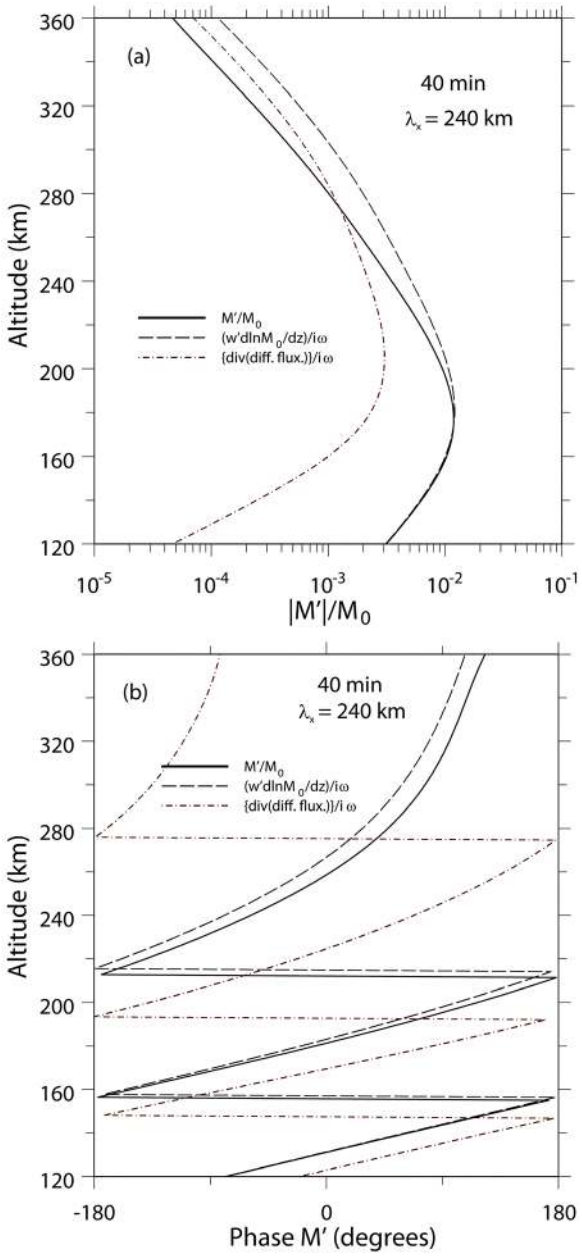

Figure 7. Same as Figure 5 except for a wave with a 40 min period and 240 km horizontal wavelength.

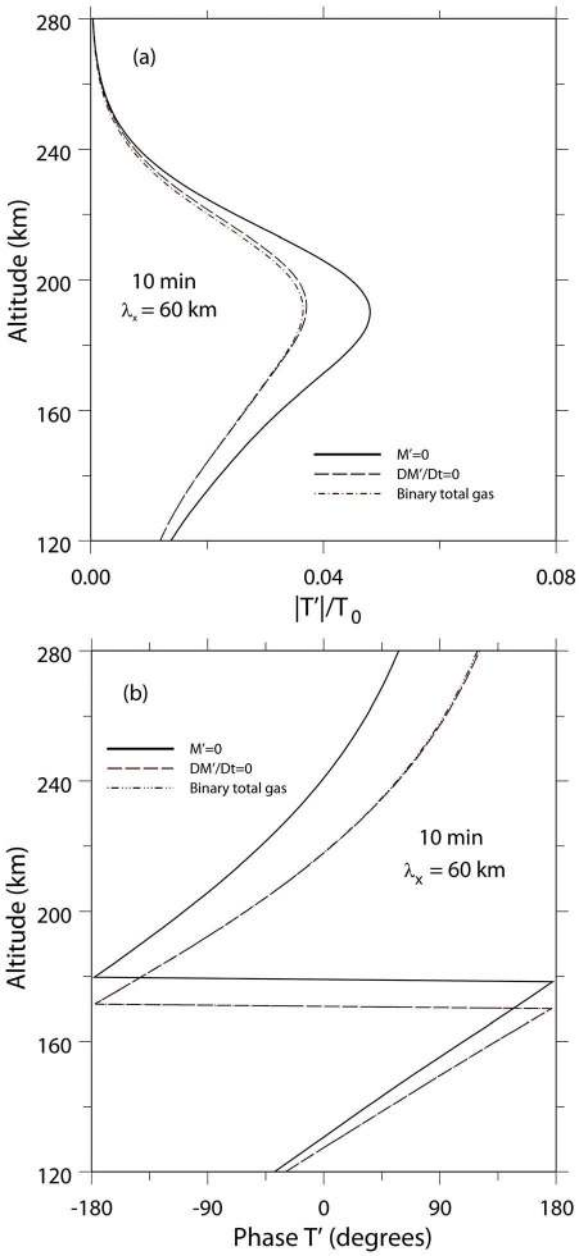

Figure 8. The (a) amplitude and (b) phase of the relative temperature fluctuation for a wave with a 10 min period and 60 km horizontal wavelength from the one-gas model with $M' = 0$ (solid), from the one-gas model where M' is nonzero based on (13) (dashed) and from the binary total gas model (dot dashed).

altitudes where the $\bar{M}$ gradient is smaller. The feature just above 120 km seen in all three solutions is where a maximum in the Brunt-Vaisala frequency is found.

[36] The phases for the $DM/Dt = 0$ solution are only slightly improved over the $M' = 0$ below the amplitude peak, but at higher altitudes the former become significantly more accurate. Similar results were found for the slower waves, but the largest relative improvements (approaching 30%) were found above the amplitude peaks.

[37] The most striking feature of the results is the very good agreement between the binary total gas results and the one-gas solutions based on the $DM/Dt = 0$ limit.

5. Discussion

[38] The effects of gravity waves on composition are given in (8). There is competition between two opposing effects: the effects of vertical advection in perturbing composition and the effects of mutual diffusion in damping the perturbation. The perturbing effects are a function of the vertical gradient of the mean molecular weight and the disturbance vertical velocity, while the latter is a function of the decoupling between the species.

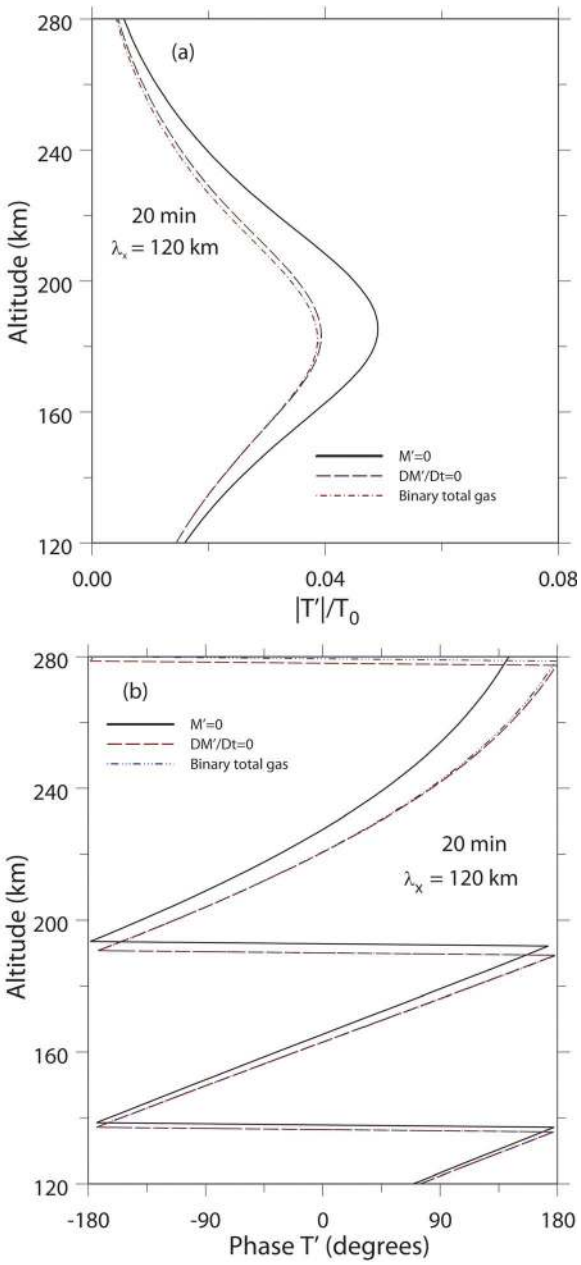

Figure 9. Same as Figure 8 except for a wave with a period of 20 min and a horizontal wavelength of 120 km.

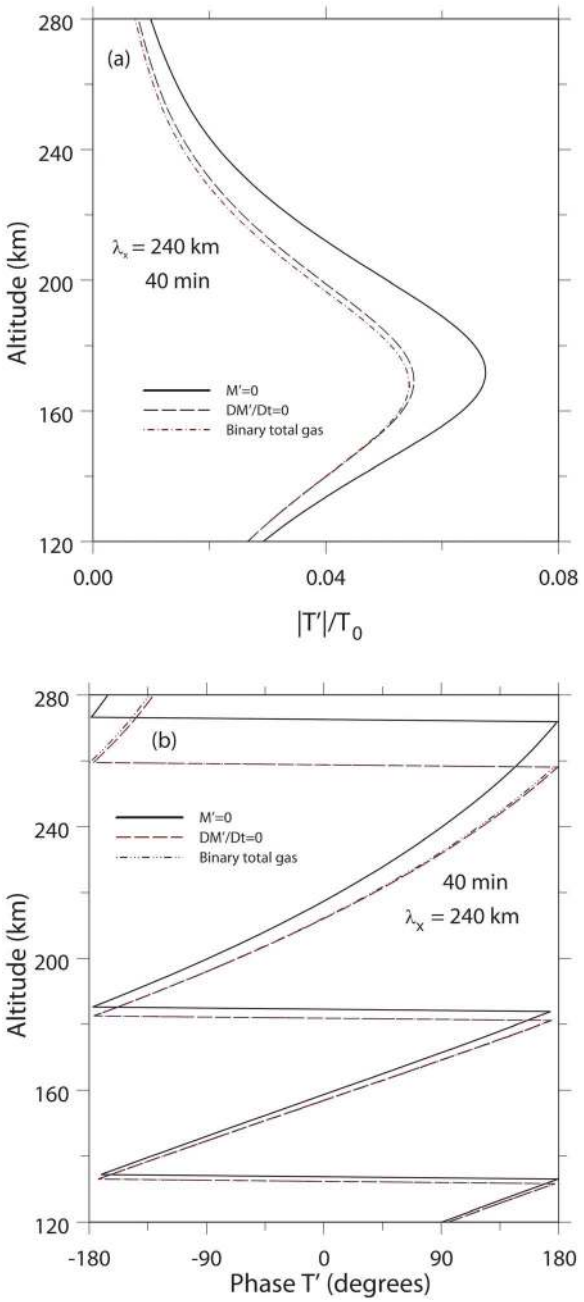

Figure 10. Same as Figure 8 except for a wave with a period of 40 min and a horizontal wavelength of 240 km.

[39] The relative contribution of vertical advection and mutual diffusion is a function of wave frequency. The longer the wave period the smaller the aspect ratio w'/u' and the smaller the contribution of the perturbing effects of gravity waves on the mean molecular weight in proportion to the forcing.

[40] Where the vertical velocities for the two species begins to decouple depends, on the one hand, on the ratio $(K_{st}/\bar{\rho}_s)/\omega$ governing the strength of the coupling, and, on the other, on tendencies for the species to act independently as the differential vertical advection acts to force them apart. The latter tendency is described by use of the wave continuity equations. At altitudes where waves are coupled to the extent that their velocities are similar, the individual continuity equations may be combined to give the advection tendency

$$\frac{\partial}{\partial t}\left(\frac{n'_O}{\bar{n}_O}-\frac{n'_{N_2}}{\bar{n}_{N_2}}\right)=w'(M_0-M_{N_2})\frac{g}{R^*\bar{T}} \tag{13}$$

The differential density perturbations are associated with differential pressure perturbations and these perturbations

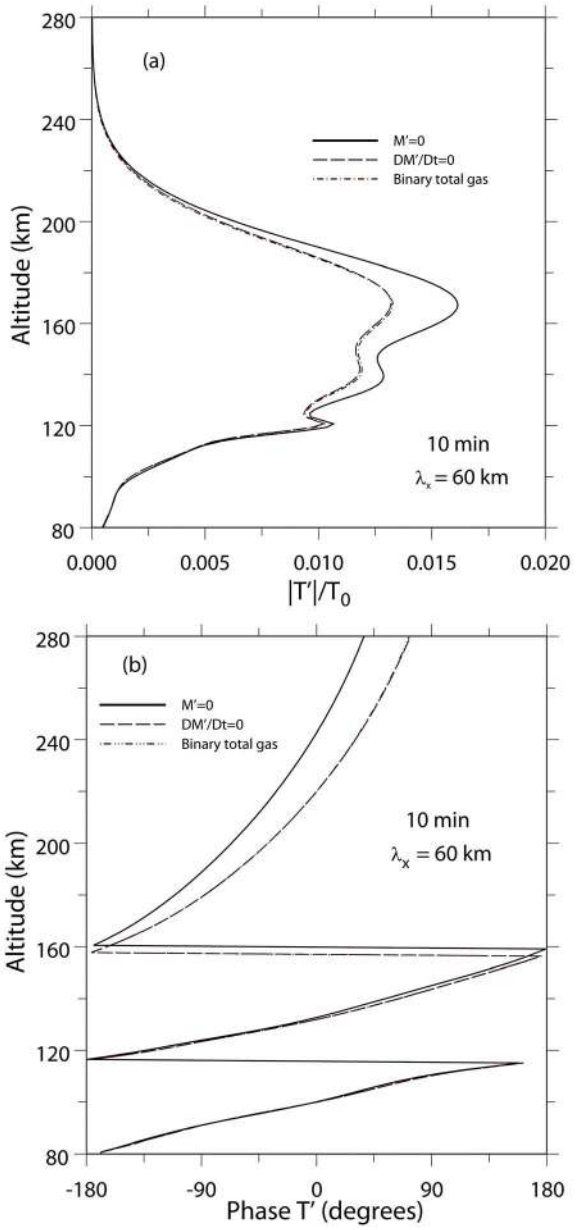

Figure 11. The (a) amplitude and (b) phase of the relative temperature fluctuation for a wave with a 10 min period and 60 km horizontal wavelength from the one-gas model with $M' = 0$ (solid), from the one-gas model where M' is nonzero based on (13) (dashed) and from the binary total gas model (dot dashed). Results are for a nonisothermal atmosphere as described in the text.

produce forces that act to increase the differential in the gas velocities for the two constituents.

[41] The competition between the perturbing effects of vertical advection on the mean molecular weight and the restoring effects of mutual diffusion are shown in Figures 5–7. These figures show the combined and separate effects of vertical advection and mutual diffusion on the relative fluctuation in mean molecular weight $M'/\bar{M}$ for 10, 20 and 40 min waves, respectively, with phase speeds of 100 $m\ s^{-1}$. In the lower thermosphere (below ~250 km) $M'/\bar{M}$ is significantly different from zero because of vertical advection. The peak in the $M'/\bar{M}$ profile occurs near 200 km for the 10 min waves and becomes progressively lower for increasing period, occurring near 180 km for the 40 min wave. This is consistent with the earlier decoupling of slow waves discussed earlier in this section. The profile of the diffusive contribution peaks about 20 km higher than the advective contribution, and decreases more slowly with height. Diffusive effects are essentially nil near and below the peak for all three waves. The contribution due to mutual diffusion becomes increasingly important with increasing altitude and is more pronounced the slower the wave. However, the advective contribution remains dominant over all altitudes considered.

[42] It is clear from the results shown in Figures 5–7 that diffusive effects do not significantly reduce $M'/\bar{M}$ perturbations in the region where they are generated by vertical advection, but may have a significant affect at higher altitudes. This is reflected in the results for $T'/\bar{T}$ shown in Figures 8–10 where it is seen that throughout much of the lower and middle thermosphere the approximation $\partial M'/\partial t = -w'\partial\bar{M}/\partial z$ is significantly more accurate than the standard approximation $M' = 0$. This confirms the earlier suggestion of *Walterscheid and Hickey* [2001]. We expect this approximation to hold for most waves that are able to propagate into the middle thermosphere without severe attenuation. This is because, except for waves with very long horizontal wavelengths, they must be fairly high frequency waves and mutual diffusion would not act fast enough to cancel the perturbing effect of the advection of mean molecular weight.

[43] The compositional effects are sensitive to the vertical gradient of the mean molecular weight. The vertical variation that we have chosen is close to the variation shown in the U.S. Standard Atmosphere, 1976 [*COESA*, 1976]. Variations at high latitudes under average solar flux conditions are much steeper and are associated with larger errors for the standard approximation (~30% at the $T'/\bar{T}$ peak) for the same 10 min wave considered here (Figure 11) [*Walterscheid and Hickey*, 2001].

6. Conclusions

[44] We have examined compositional effects on the total gas results and compared them with a one-gas model where mean molecular weight is either held constant (the standard approximation) or conserved following a parcel [*Walterscheid and Hickey*, 2001]. There are two limiting cases. The first is where composition does not respond to wave motion and the other where it responds to wave motion as if composition were a conserved quantity. These may be incorporated into a one-gas model by requiring respectively that $M' = 0$ or $\partial M'/\partial t = -w'\partial\bar{M}/\partial z$. We find that compositional effects are significant and that conservation of mean molecular weight is a significantly better approximation than the standard approximation. Indeed, if it is the total gas response that is of interest one does not need to use a multiconstituent model, rather a one-gas model that includes conservation of mean molecular weight is adequate. A significant compositional effect is the fact that the viscosity and thermal conduction of a given species are reduced by the presence of another species.

[45] **Acknowledgments.** M.P.H. was supported by the National Science Foundation under grant ATM-0639293. R.L.W. was supported by a subcontract to Embry-Riddle Aeronautical University under NSF grant ATM-0639293. R.L.W. also acknowledges support by NASA grants NNX08AM13G and NNX11AH82G and by NSF grant AGS1001086.

[46] Robert Lysak thanks the reviewers for their assistance in evaluating this paper.

References

Brinkman, D. G., R. L. Walterscheid, L. R. Lyons, D. C. Kayser, and A. B. Christensen (1995), *E* region neutral winds in the post-midnight diffuse aurora during the ARIA I rocket campaign, *J. Geophys. Res.*, *100*, 17,309–17,320, doi:10.1029/94JA02814.

Bruce, G. H., D. W. Peaceman, H. H. Rachford Jr., and J. D. Rice (1953), Calculations of unsteady-state gas flow through porous media, *Petrol. Trans. AIME*, *198*, 79–92.

Burgers, J. M. (1969), *Flow Equations for Composite Gases*, Academic, San Diego, Calif.

COESA (1976), *U.S. Standard Atmosphere*, 227 pp., Gov. Print. Off., Washington, D. C.

Colegrove, F. D., F. S. Johnson, and W. B. Hanson (1966), Atmospheric composition in the lower thermosphere, *J. Geophys. Res.*, *71*, 2227–2236.

Del Genio, A. D. (1978), Characteristics of acoustic gravity waves in a diffusively separated atmosphere, Ph.D. diss., Univ. of Calif., Los Angeles.

Del Genio, A. D., G. Schubert, and J. M. Straus (1979a), Characteristics of acoustic-gravity waves in a diffusively separated atmosphere, *J. Geophys. Res.*, *84*, 1865–1879, doi:10.1029/JA084iA05p01865.

Del Genio, A. D., G. Schubert, and J. M. Straus (1979b), Gravity wave propagation in a diffusively separated atmosphere with height-dependent collision frequencies, *J. Geophys. Res.*, *84*, 4371–4378, doi:10.1029/JA084iA08p04371.

Dickinson, R. E., E. C. Ridley, and R. G. Roble (1984), Thermospheric general circulation with coupled dynamics and composition, *J. Atmos. Sci.*, *41*, 205–219, doi:10.1175/1520-0469(1984)041<0205:TGCWCD>2.0.CO;2.

Fuller-Rowell, T. J., and D. Rees (1981), A three-dimensional time-dependent simulation of the global dynamical response of the thermosphere to a geomagnetic substorm, *J. Atmos. Terr. Phys.*, *43*, 701–721, doi:10.1016/0021-9169(81)90142-2.

Hagan, M. E., M. D. Burrage, J. M. Forbes, J. Hackney, W. J. Randel, and X. Zhang (1999), GSWM-98: Results for migrating solar tides, *J. Geophys. Res.*, *104*, 6813–6827, doi:10.1029/1998JA900125.

Hays, P. B., R. A. Jones, and M. H. Rees (1973), Auroral heating and the composition of the neutral atmosphere, *Planet. Space Sci.*, *21*, 559–573, doi:10.1016/0032-0633(73)90070-6.

Hedin, A. E. (1991), Extension of the MSIS thermospheric model into the middle and lower atmosphere, *J. Geophys. Res.*, *96*, 1159–1172, doi:10.1029/90JA02125.

Herning, F., and L. Zipperer (1936), Calculation of the viscosity of technical gas mixtures from viscosity of the individual components, *Gas Wasserfach.*, *79*, 69–73.

Hickey, M. P., and K. D. Cole (1987), A quartic dispersion equation for internal gravity waves in the thermosphere, *J. Atmos. Terr. Phys.*, *49*, 889–899, doi:10.1016/0021-9169(87)90003-1.

Hickey, M. P., R. L. Walterscheid, M. J. Taylor, W. Ward, G. Schubert, Q. Zhou, F. Garcia, M. C. Kelley, and G. G. Shepherd (1997), Numerical simulations of gravity waves imaged over Arecibo during the 10-day January 1993 campaign, *J. Geophys. Res.*, *102*, 11,475–11,489, doi:10.1029/97JA00181.

Hickey, M. P., R. L. Walterscheid, and G. Schubert (2000), Gravity wave heating and cooling in Jupiter's thermosphere, *Icarus*, *148*, 266, doi:10.1006/icar.2000.6472.

Kittel, C. (1969), *Thermal Physics*, 418 pp., John Wiley, Hoboken, N. J.

Lindzen, R. S., and H. L. Kuo (1969), A reliable method for the numerical integration of a large class of ordinary and partial differential equations,

Mon. Weather Rev., *97*, 732–734, doi:10.1175/1520-0493(1969)097<0732:ARMFTN>2.3.CO;2.

Mayer, H. G., I. Harris, and N. W. Spencer (1978), Some properties of upper atmospheric helium, *Rev. Geophys.*, *16*, 539–565, doi:10.1029/RG016i004p00539.

Mayr, H. G., I. Harris, F. Varosi, and F. A. Herrero (1984), Global excitation of wave phenomena in a dissipative multiconstituent medium: 1. Transfer function of the Earth's thermosphere, *J. Geophys. Res.*, *89*, 10,929–10,959, doi:10.1029/JA092iA07p07657.

Mayr, H. G., I. Harris, F. Varosi, and F. A. Herrero (1987), Global excitation of wave phenomena in a dissipative multiconstituent medium: 3. Response characteristics for different sources in the Earth's thermosphere, *J. Geophys. Res.*, *92*, 7657–7672, doi:10.1029/JA092iA07p07657.

Mikkelsen, I. S., and M. F. Larsen (1991), A numerical modeling study of the interaction between the tides and the circulation forced by high-latitude plasma convection, *J. Geophys. Res.*, *96*, 1203–1213, doi:10.1029/90JA01869.

Mikkelsen, I. S., T. S. Jorgensen, M. C. Kelley, M. F. Larsen, and E. Perira (1981), Neutral winds and electric fields in the dusk auroral oval, 2, theory and model, *J. Geophys. Res.*, *86*, 1525–1536, doi:10.1029/JA086iA03p01525.

Reber, C. A., and P. B. Hays (1973), Thermospheric wind effects on the distribution of helium and argon in the Earth's upper atmosphere, *J. Geophys. Res.*, *78*, 2977–2991, doi:10.1029/JA078i016p02977.

Richmond, A. D., and S. Matsushita (1975), Thermospheric response to a magnetic substorm, *J. Geophys. Res.*, *80*, 2389–2850, doi:10.1029/JA080i019p02839.

Schubert, G., M. P. Hickey, and R. L. Walterscheid (2003), Heating of Jupiter's thermosphere by the dissipation of upward propagating acoustic waves, *Icarus*, *163*, 398–413, doi:10.1016/S0019-1035(03)00078-2.

Schunk, R. W. (1977), Mathematical structure of transport equations for multispecies flows, *Rev. Geophys.*, *15*, 429–445, doi:10.1029/RG015i004p00429.

Straus, J. M., S. P. Creekmore, and B. K. Ching (1977), A dynamical model of upper atmosphere helium, *J. Geophys. Res.*, *82*, 2132–2138, doi:10.1029/JA082i016p02132.

Sun, Z.-P., R. P. Turco, R. L. Walterscheid, S. V. Venkateswaran, and P. W. Jones (1995), Thermospheric response to morningside diffuse aurora: High-resolution three-dimensional simulations, *J. Geophys. Res.*, *100*, 23,779–23,793, doi:10.1029/95JA02298.

Walterscheid, R. L., and M. P. Hickey (2001), One-gas models with height-dependent mean molecular weight: Effects on gravity wave propagation, *J. Geophys. Res.*, *106*, 28,831–28,839, doi:10.1029/2001JA000102.

Walterscheid, R. L., L. R. Lyons, and K. E. Taylor (1985), The perturbed neutral circulation in the vicinity of a symmetric stable auroral arc, *J. Geophys. Res.*, *90*, 12,235–12,248, doi:10.1029/JA090iA12p12235.

M. P. Hickey, Department of Physical Sciences, Embry-Riddle Aeronautical University, 600 S. Clyde Morris Blvd., Daytona Beach, FL 32114, USA. (michael.hickey@erau.edu)

R. L. Walterscheid, Space Science Applications Laboratory, M2-260, The Aerospace Corporation, 2350 East El Segundo Blvd., El Segundo, CA 90245-4691, USA. (richard.walterscheid@aero.org)